



NIR-II Fluorescence Imaging Using Indocyanine Green Provides Early Prediction of Skin Avulsion-Injury in a Porcine Model

Siqi Gao*, Yifeng Yu*, Zheng Wang, Yifan Wu, Xingan Qiu , Chao Jian, Aixi Yu 

Department of Orthopedics Trauma and Microsurgery, Zhongnan Hospital of Wuhan University, Wuhan, Hubei, 430071, People's Republic of China

*These authors contributed equally to this work

Correspondence: Aixi Yu; Chao Jian, Department of Orthopedics Trauma and Microsurgery, Zhongnan Hospital of Wuhan University, Wuhan, Hubei, 430071, People's Republic of China, Tel +86-27-6781-3120; +86-27-6781-3120, Email yuaixi@whu.edu.cn; chaojian@whu.edu.cn

Purpose: Currently, skin avulsion-injury reconstruction is mainly based on subjective evaluation of traditional clinical signs. It frequently results in unnecessary tissue loss and incomplete debridement-related infection. This pilot study aimed to develop a novel near-infrared (NIR) II fluorescence imaging method to assess avulsed skin-perfusion status and thus predict its outcome early.

Methods: Skin avulsion-injury models were established by avulsing 10×4 cm pedicled flaps on porcine hindlimbs. A clinically available improved NIR-I/II multispectral imaging system was applied for NIR imaging using indocyanine green (ICG) fluorescence. Continuous NIR-wavelength filters and dynamic imaging were used to investigate optimal imaging conditions and time window. NIR-I/II imaging was synchronously conducted for quality comparison of the two methods. Visual inspection and histological studies were used for assessing the final outcome of avulsed skin.

Results: NIR-II fluorescence imaging with a 1,100 nm filter obtained satisfactory performance and reached maximum fluorescence intensity at 1 minute after ICG injection. NIR-II imaging clearly visualized the microvascular network in vascularized avulsed skin and revealed “dark areas” in nonvascularized avulsed skin in a real-time fashion. NIR-II fluorescence imaging demonstrated higher resolution than NIR-I imaging, as indicated by a higher signal-to-background ratio (2.11) and lower full width at half maximum (6.50614). The dark area of avulsed skin on imaging finally developed to necroses that were confirmed by histology.

Conclusion: NIR-II real-time fluorescence imaging clearly maps the microvascular network and shows the perfusion status of avulsed skin at higher resolution than traditional NIR-I imaging, and thus precisely predicts the outcome of avulsed skin early.

Keywords: ICG, near-infrared fluorescence imaging, skin avulsion-injury, swine model

Introduction

Skin avulsion-injury is caused by strong shear and friction force resulting in the skin and subcutaneous tissue separating from the deep fascia, normally forming pedicled avulsion flaps connected with the limbs.^{1–3} It has been classified into four patterns: abrasion/avulsion, noncircumferential degloving, circumferential single-plane degloving, and circumferential multiplane degloving.⁴ In most cases, avulsed tissue were used in reconstruction. However, up to 86.8% cases suffer partial or even complete tissue loss. As insufficient or compromised blood supply is not well evaluated in initial debridement, avascular tissue is be debrided, which predisposes the wounds to infection. The resulting necroses also need additional procedures. Avulsed skin processing into split-thickness grafts is a frequently used coverage option, but is not favored due to its poor appearance and functional outcomes especially for planta- and palm-skin avulsion. Theoretically, a residual pedicle or revascularization strategy enables at least partial avulsed tissue survival, and thus can be preserved and used directly for reconstruction. In addition, the other avascular skin retains viable cells that can be debrided and serve as a source of skin graft for the remaining coverage. In this regard, making full use of the affected skin allows for the injury succumbing to a one-stage procedure and obtaining an optimal reconstructive outcome.

In order to economically utilize the avulsed skin for reconstruction and avoid unnecessary complications and additional procedures, precise identification of the boundary between the perfusion area and nonperfusion area is a prerequisite. Currently, clinical evaluation of the perfusion status of an avulsed skin flap is mainly determined by visual inspection, eg, skin color, cutaneous bleeding, and capillary refill, but these largely depend on a surgeon's experience and are not accurate in predicting the outcome of the avulsed skin.^{5–7} Near-infrared (NIR)-fluorescence imaging is widely used to visualize many biological processes due to its advantages of nonionization, real-time imaging, high sensitivity, and resolution.^{8–11} It can be divided into an NIR-I window (700–900 nm) and an NIR-II window (900–1,700 nm) based on emission wavelength. A growing number of studies have shown that NIR-II image quality is superior to NIR-I in diagnostic imaging and imaging-guided surgery, as indicated by its higher resolution and sensitivity, deeper penetration, and less autofluorescence and light scattering.^{12–14} In one study, NIR-II imaging was employed to image avulsed skin in a small-animal model and succeeded in accurately predicting necrotic margins.¹⁵ However, the imaging equipment and probes are not suitable for a clinical setting. Recently, an integrated visible and NIR-I/II multispectral imaging instrument was developed and used clinically for imaging-guided liver-tumor surgery.¹⁶ This instrument has since been improved upon and retains excellent imaging performance.

Motivated by advancements in NIR fluorescence-imaging instrumentation and clinically ready-to-use NIR-I/II fluorescent indocyanine green (ICG), we designed this study to investigate the feasibility of the novel multispectral fluorescence imaging for assessing perfusion status of avulsed skin and the accuracy of its early necrosis-margin prediction and to compare the imaging quality of the NIR-II window with the NIR-I window. We used a porcine model to yield highly clinically relevant outcomes, eventually providing a profile for translating this technique to clinical use, including imaging-guided radical debridement and reconstruction in skin avulsion-injury.

Methods

NIR Fluorescence-Imaging System

Based on the first-generation visible NIR-I/NIR-II integrated imaging system, an NIR-II imaging system was developed for better clinical application.¹⁶ As shown in [Figure 1](#), it has the merits of portability, light weight (4 kg), and ease of operation. An InGaAs camera (640×512 pixels, TE4-25; Hengxin, Shenyang, China) cooled to -80°C was utilized to capture images in the NIR-II window. According to the experimental requirements, NIR-II fluorescence signals were able to be extracted by various long-pass filters. For example, were a 1,100 nm image needed, we would fit a 1,100 nm long-pass filter (ThorLabs, Newtown, NJ, USA) to the camera, limiting wavelength $<1,100$ nm to pass through the lens. A silicon camera (1,920×1,080 pixels, CS2100M; ThorLabs, Newtown, NJ, USA) equipped with a 900 nm short-pass filter was used to acquire images in the NIR-I window. In both NIR-I window and NIR-II window fluorescence imaging, a 785 nm laser (Ningbo Yuanming Laser Technology, Zhejiang, China) beam was exploited to provide uniform illumination extended through a lens on the region of interest (ROI), and the excitation wavelength was filtered away by 800 nm long-pass filters. The facular power density was consistently adjusted to 10–15 mW/cm² during testing.

Experimental Animals

We purchased male landrace pigs aged 12–14 weeks and weighing 25–30 kg from the Laboratory Animal Center of Wuhan University (Hubei, China). All surgeries and clinical assessments were performed by three surgeons. The experimental procedures, including both operation and measurements, were performed under general anesthesia with propofol (0.3 mg/kg/h body weight). After the operation, pigs received analgesic therapy with 0.4 mg/kg/day meloxicam for 7 days via intramuscular injection. All pigs were euthanized with an overdose sodium pentobarbital at the end of the study. All efforts were made to minimize animal suffering. Our experiments were performed in compliance with the guidelines of the Institutional Animal Care and Use Committee of Wuhan University. The experimental protocol was approved by the Experimental Animal Welfare Ethics Committee of Zhongnan Hospital of Wuhan University (approval ZN2021069, Wuhan, China).



Figure 1 NIR-I/II fluorescence imaging system used for in vivo NIR fluorescence imaging in porcine limbs.

Establishment of the Porcine Model

Eight pigs were used to establish the skin avulsion–injury model. The anesthetized pig was placed in prone position, limbs stretched and fixed, and hindlimbs shaved gently with an electric razor and sterilized with povidone iodine. In order to establish a replicable avulsed-skin model with partial necrosis, a full-thickness triangle (10×4 cm) skin flap on the hindlimb was selected according to our preliminary experiments. After the flap had been mapped, a full-thickness skin incision was made along the marker to assure the flap had relatively constant area and position, and then the tip of the skin flap was fixed with a vessel clamp, avulsed proximally, and pulled for 15 minutes. The obvious vessels entering the flap were avulsed or cut. After the skin injury, it was intermittently sutured to the original position with nylon 5–0. All this performed by the same group of surgeons strictly following aseptic procedures.

In Vivo NIR-Fluorescence Imaging

ICG (0.5 mg/kg; Dandong Pharmaceutical Factory, Liaoning, China) was injected into the anesthetized pigs via the ear vein. Firstly, fluorescence images of avulsed skin flaps were collected progressively using 900, 1,000, 1,100, 1,200, and 1,300 nm long-pass filters in the NIR-II window. High-quality images were chosen, then porcine-skin metabolism was observed under imaging in NIR-II and NIR-I windows. Both NIR-II and NIR-I fluorescence–imaging acquisition happened before surgery and dynamic observation 1 hour after surgery. “Dark areas” of distal flaps can be seen as predictive of necrosis. Each pig was placed in a separated cage in an air-conditioned room after observation and fed a standard laboratory diet for 7 days. This duration was sufficient to expose clinical necrosis in avulsed flaps. Digital photographs were taken before surgery and on postoperative day (POD) 7 to confirm necrosis of the avulsed skin.

Histological Study

After 7 days’ observation, samples of avulsed flaps were collected and subjected to histological examination with H&E and Masson trichrome staining. Cell morphology and tissue structure were qualitatively interpreted using 10× magnification images.

Data Analysis

ImageJ 1.8.0 was used to measure mean signal intensity in ROIs to quantitatively analyze each fluorescent image. Graphs were generated by OriginPro 9.5.0. Data are represented as means \pm SD. Student's *t*-test was used for statistical analysis. Skin-necrosis area was assessed based on 7 days' digital photos by three surgeons based on clinical signs (dehydration, eschar formation, and incrustation).

Results

Determination of Optimal Filter for NIR-II Imaging

To explore optimal imaging conditions for skin avulsion-injury, a series of 900, 1,000, 1,100, 1,200, and 1,300 nm NIR-II fluorescence images of ROIs were taken. As shown in Figure 2, with increase wavelength, background signals around vessels were weakened, but longer exposure was required to capture suitable images. Skin microvascular network structure was displayed clearly with better spatial resolution and higher fluorescence intensity through the 1,100 nm long-pass filter than the other filters. Therefore, the 1,100 nm long-pass filter was selected for subsequent study.

Dynamic NIR-II Fluorescence Imaging

To investigate the best time window for image capture, real-time NIR-II fluorescence imaging was conducted. Normal skin in the same location was imaged for comparison (Figure 3A). Figure 3B shows the dynamic NIR-II imaging achieved with the 1,100 nm long-pass filter. When ICG was injected into the vein, the vessels became visible within seconds, fluorescence intensity increased rapidly and peaked at about 1 minute, then gradually decreased to the baseline level about 30 minutes after injection (Figure 3C). In contrast to the normal-skin image in Figure 3A, the distal end of the avulsed skin constantly failed to light up, as shown in the "dark areas" during real-time monitoring. These areas implied loss of perfusion and a forecast of necrosis.

Comparison of NIR-I and NIR-II Imaging Quality

NIR-I and NIR-II fluorescence imaging were simultaneously performed on same ROI at 800 nm and 1,100 nm wavelength, respectively. Both modalities demonstrated similar "dark areas" (Figure 4A and B) at 1 hour after the

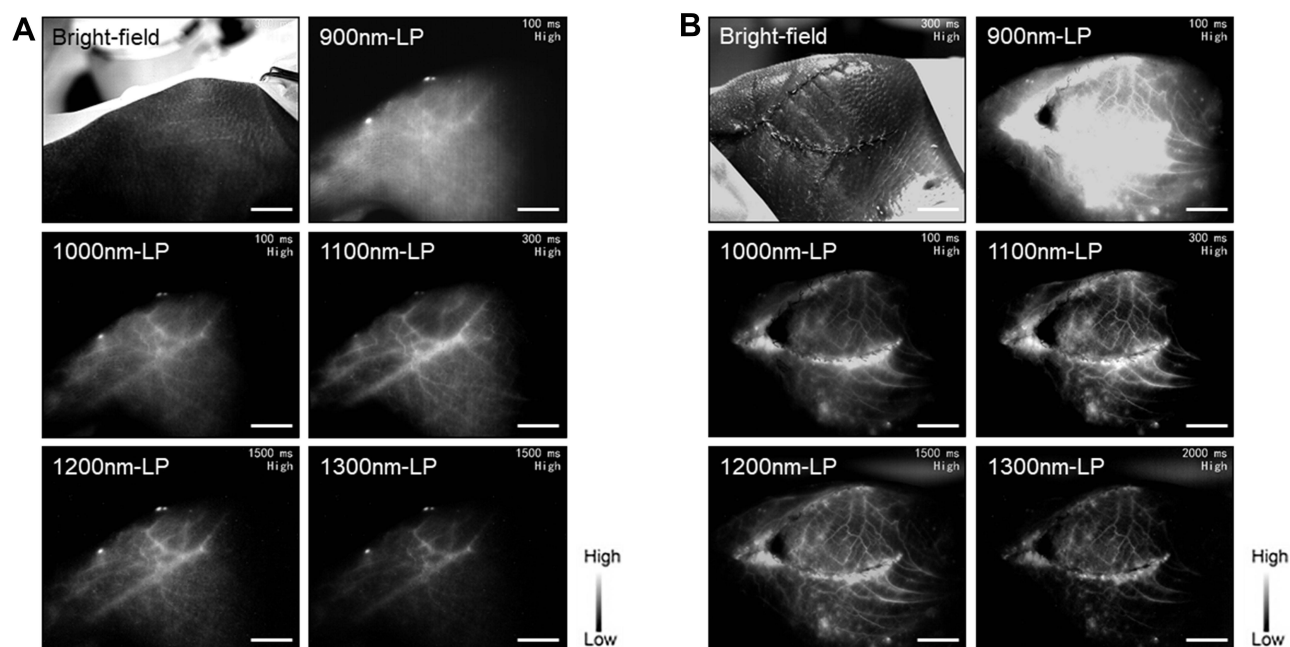


Figure 2 Optimal imaging conditions for skin avulsion-injury. Bright-field and NIR-II fluorescence images with 900, 1,000, 1,100, 1,200, and 1,300 nm long-pass filters of preoperation (A) and postoperation (B) ROIs in porcine limbs. Bars 3 cm.

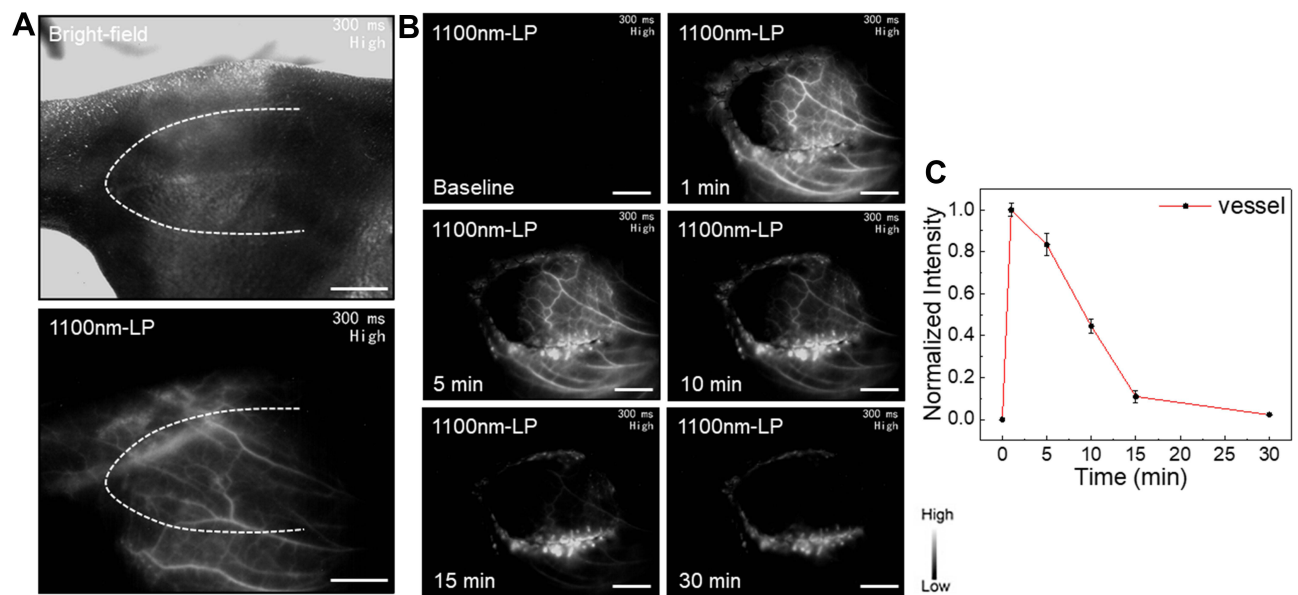


Figure 3 Best time window for capturing images of skin avulsion-injury. (A) Bright-field (upper) and NIR-II fluorescence (lower) images of normal skin in porcine limbs. (B) Dynamic fluorescence imaging 0–30 minutes after intravenous injection of ICG. (C) Dynamic fluorescence-intensity measurement of skin blood vessel 0–30 minutes after intravenous injection of ICG. Bars 3 cm.

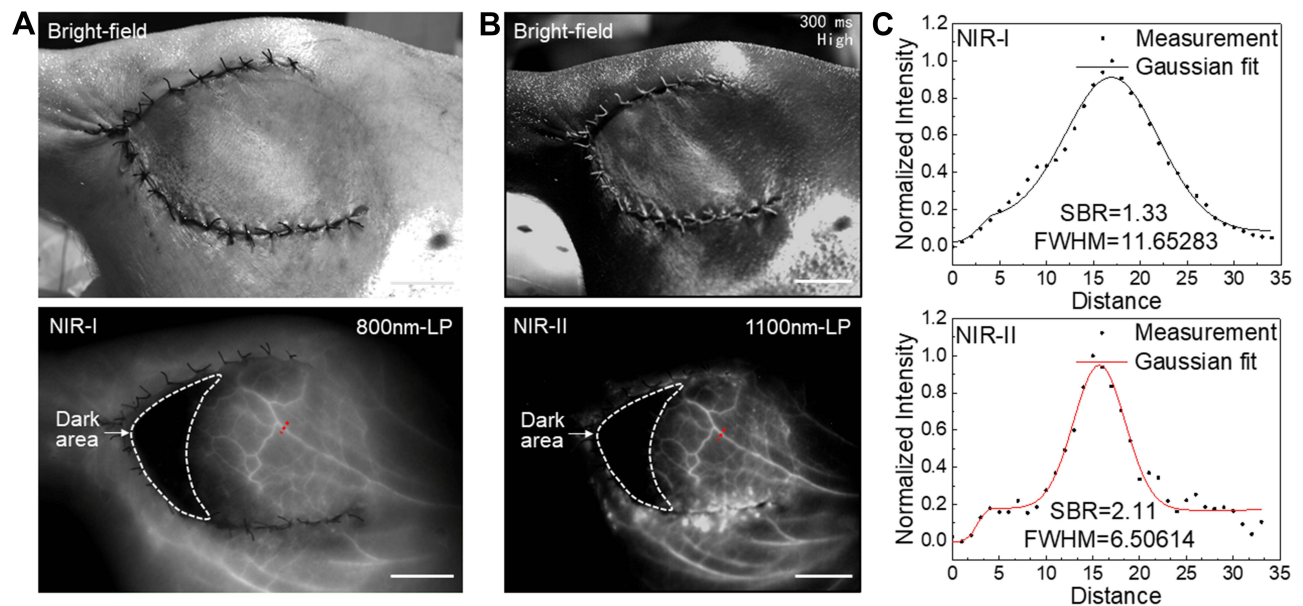


Figure 4 Imaging qualities of NIR-I/II fluorescence in skin avulsion-injury. (A) Bright-field (upper) and NIR-I fluorescence (lower) images of avulsed hindlimb flap at 1 hour after the operation. (B) Bright-field (upper) and NIR-II fluorescence (lower) images of avulsed hindlimb flap. (C) Cross-sectional NIR-I (upper) and NIR-II (lower) fluorescence distribution along the red dotted line of the blood vessel. Gaussian fit to the distribution is shown as the solid line in each image. Bars 3 cm.

operation. In NIR-II imaging (Figure 4B), the vascular network was easily identified with excellent contrast, exceeding that on NIR-I (Figure 4A). The FWHM of two Gaussian fitting terms to the intensity distribution along the red dotted line were calculated as 6.50614 on NIR-II imaging and 11.65283 on NIR-I imaging. SBRs were 2.11 on NIR-II imaging and 1.33 on NIR-I imaging (Figure 4C). These parameters revealed that NIR-II imaging had significantly higher resolution than the NIR-I imaging.

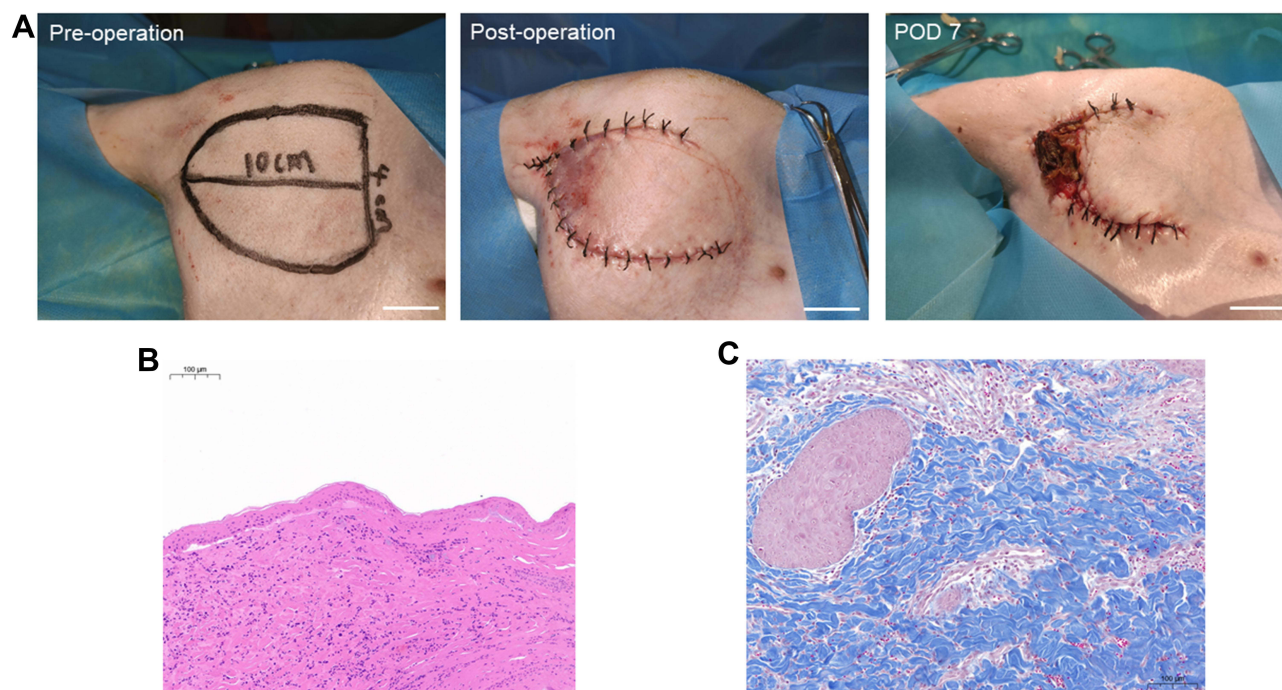


Figure 5 Clinical potential of NIR-II fluorescence imaging in early prediction of tissue necrosis of skin avulsion-injuries. (A) Digital images of preoperation (left), postoperation (middle), and on POD7 (right) of avulsed flap of porcine hindlimb. (B) H&E staining of “dark area” skin of avulsed hindlimb flap on POD7. (C) Masson's trichrome staining of “dark area” skin of avulsed hindlimb flap on POD7. Bars 3 cm (A), 0.1 mm (B,C).

Application of NIR-II Imaging in Early Prediction of Skin Avulsion–Injury Outcome

To further verify the potential and accuracy of NIR-II fluorescence imaging in early prediction of skin necrosis in avulsion injuries, the status of avulsed skin was observed until POD7. As shown in Figure 5, complete necrosis of distal avulsed flaps was obvious and confirmed by H&E staining on POD7. The final necrosis area was in line with the dark area through the suture marker. This showed that NIR-II imaging can precisely predict the final outcome of avulsed skin early.

Discussion

Given optical imaging depth is confined to centimeters' thickness of tissue, most underlying organs need be dissected to be directly exposed for imaging, and thus these optical imaging techniques are optimally indicated for intraoperative use and especially for clinical use. The skin is a body-surface organ, facilitating imaging without any surgical procedures and affording real-time monitoring of perfusion status. The thickness of the avulsed skin fits imaging depths exactly. Additionally, porcine skin is similar to human skin, both histologically and ultrastructurally.¹⁷ In preliminary experiments, we attempted to establish avulsion flaps in the anterior tibial area, which is more common in clinical practice. However, the high incidence of infections and wound dehiscence and poor animal compliance often led to experimental failure. As a result, the medial hindlimb was selected for model establishment. In the clinical setting, many avulsed-skin samples can survive intact via in situ suturing and drug administration.¹⁸ Abundant perforators in this area probably served as pedicles sufficient to supply the avulsed flap in this porcine model. In order to generate a stable partial-necrosis model, four measures were taken. Firstly, the obvious vessels entering the flap were avulsed or cut. Secondly, the flap was designed with high length:width ratio (2.5:1), which exceeded that of random flap-design limits. Flaps were triangular instead of rectangular. Thirdly, the avulsed flap retained some subcutaneous tissue which could avoid the flap directly nourished by the underlying tissue. Finally, the flap was avulsed quickly and then pulled for 15 minutes, which perhaps destroyed the microvascular network. These measures were validated to effectively establish a replicable partial-necrosis model in the preliminary study and used for subsequent experiments. As this was a pilot study, we selected a relatively simple pattern of degloved/avulsed skin injury. Nevertheless, these injuries frequently couple with crushing and rolling

injuries, have greater area and multiple-plane injury, or are complicated by bone and tendon exposure. Due to the model's limitations, the results were not all-encompassing, and thus further studies need to be conducted in other clinically relevant scenarios.

NIR-II imaging with a 1,100 nm long-pass filter obtained satisfactory imaging performance. It clearly visualized the vascular network of vascularized avulsed skin with high spatial resolution, while nonvascularized avulsed skin was not lit up, providing a basis for forecasting the outcome of avulsed skin. During postoperative observations, the dark areas developed to necroses, which were confirmed by histological study. Based on ICG's perfusion-dependent distribution, fluorescence intensity peaked at 1 minute after injection. This is consistent with a previous human ICG-based visible fluorescence-imaging study.^{19,20}

NIR-I/II fluorescence imaging was conducted simultaneously at 800 nm and 1,100 nm wavelengths, respectively. The two imaging methods demonstrated similar dark area and showed comparable capacity for early prediction of avulsed-skin necrosis. However, NIR-II imaging presented more distinct microvascular structures and higher resolution in perfused zones of avulsed skin than NIR-I imaging. NIR-II imaging had relatively higher SBR (2.11) and relatively lower FWHM (11.65) than NIR-I imaging (1.33 and 6.51). Additionally, it was verified that NIR-II imaging revealed more tissue depth than NIR-I imaging.¹⁶ All these findings indicated that NIR-II fluorescence imaging possesses better performance than the more frequently used NIR-I fluorescence imaging, due to its reduced tissue autofluorescence, reduced photon scattering, and the low level of photon absorption at longer wavelengths.^{21,22} Despite similar effects on necrosis-area prediction, NIR-II imaging might have greater value than NIR-I imaging in early evaluation of microvascular diseases, such as peripheral vascular diseases and diabetic foot, as these diseases present compromised but not absent microcirculation and affect relatively deeper tissue in the early stages. This needs to be further tested in future research.

To make this imaging technique more accessible to clinical translation, ICG was used as nontarget fluorescence without any modification. Nevertheless, its perfusion difference-predominant imaging mechanism makes ICG-based imaging sufficient to manifest significant target-to-background contrast in the skin avulsion-injury setting. Notably, it has been reported that ICG-based NIR-II imaging presents relatively lower sensitivity than NIR-I imaging. This is mainly because ICG's fluorescence-emission intensity can reach its maximum in the NIR-I window, but not in the NIR-II window.^{16,23} In this regard, it is crucial and urgent to develop clinically available probes to further improve the quality of NIR-II imaging.

The major benefit of NIR-II imaging in avulsed skin is providing reliable evidence for decision-making in debridement and reconstruction. Specifically, vascularized parts can preserve complete tissue structure for reconstruction, assuring aesthetic and functional results. Alternatively, vascular parts can be designed for local transfer to cover key structures, such as bone, tendon, and neurovascular components. Nonvascularized parts could be processed to split-thickness skin for grafts in the initial surgery, which would avoid waste. This provides an optimal reconstructive strategy and decreases hospital length of stay and cost.

Conclusion

We employed a clinically available improved NIR-I/II multispectral imaging system for NIR-fluorescence imaging of skin avulsion-injury in a porcine model. NIR-II fluorescence imaging clearly mapped the microvascular network and perfusion status of avulsed skin with higher imaging resolution than traditional NIR-I imaging, and thus precisely predicts the outcome of avulsed skin early. It holds potential clinical value for optimizing decision-making and guiding surgery, thereby achieving optimal outcomes and reducing patient burden in skin avulsion-injury.

Acknowledgments

This study was supported by the Hubei Province Training Object of the Second Session of Leading Medical Talents Project (LJ20200405) and Science and Technology Innovation Platform Project of Zhongnan Hospital of Wuhan University (PTXM2021020). Siqi Gao and Yifeng Yu are co-first authors for this study.

Disclosure

The authors report no conflicts of interest in this work.

References

1. Jeng SF, Hsieh CH, Lin TS, Kuo YR, Wei FC. Classification and reconstruction options in foot plantar skin avulsion injuries: follow-up. *Plast Reconstr Surg*. 2003;112(1):220–221. doi:10.1097/01.PRS.0000066384.90361.5C
2. Weinand C. Degloving injuries of upper extremity: a strategy with full thickness skin mesh. *World J Plast Surg*. 2018;7(3):372–376. doi:10.29252/wjps.7.3.372
3. Hu FX, Hu XX, Yang XL, et al. Treatment of large avulsion injury in perianal, sacral, and perineal regions by island flaps or skin graft combined with vacuum assisted closure. *Bmc Surg*. 2019;19(1):65. doi:10.1186/s12893-019-0529-1
4. Arnez ZM, Khan U, Tyler MP. Classification of soft-tissue degloving in limb Trauma. *J Plast Reconstr Aesthet Surg*. 2010;63(11):1865–1869. doi:10.1016/j.bjps.2009.11.029
5. Ozer K, Colak O. Discussion on the effect of omeprazole usage on the viability of random pattern skin flaps in rats. *Ann Plast Surg*. 2018;80(1):92. doi:10.1097/SAP.0000000000001166
6. Olingy CE, San EC, Ogle ME, et al. Non-classical monocytes are biased progenitors of wound healing macrophages during soft tissue injury. *Sci Rep*. 2017;7(1):447. doi:10.1038/s41598-017-00477-1
7. Matsui A, Lee BT, Winer JH, Laurence RG, Frangioni JV. Predictive capability of near-infrared fluorescence angiography in submental perforator flap survival. *Plast Reconstr Surg*. 2010;126(5):1518–1527. doi:10.1097/PRS.0b013e3181ef8ce7
8. Li T, Li C, Ruan Z, et al. Polypeptide-conjugated second near-infrared organic fluorophore for image-guided photothermal therapy. *Acs Nano*. 2019;13(3):3691–3702. doi:10.1021/acsnano.9b00452
9. Lin J, Zeng X, Xiao Y, et al. Novel near-infrared II aggregation-induced emission dots for in vivo bioimaging. *Chem Sci*. 2019;10(4):1219–1226. doi:10.1039/C8SC04363A
10. Hong G, Lee JC, Robinson JT, et al. Multifunctional in vivo vascular imaging using near-infrared II fluorescence. *Nat Med*. 2012;18(12):1841–1846. doi:10.1038/nm.2995
11. Wan H, Du H, Wang F, Dai H. Molecular imaging in the second near-infrared window. *Adv Funct Mater*. 2019;29(25):1900566. doi:10.1002/adfm.201900566
12. Li D, He S, Wu Y, et al. Excretable lanthanide nanoparticle for biomedical imaging and surgical navigation in the second near-infrared window. *Adv Sci*. 2019;6(23):1902042. doi:10.1002/advs.201902042
13. Shou K, Tang Y, Chen H, et al. Diketopyrrolopyrrole-based semiconducting polymer nanoparticles for in vivo second near-infrared window imaging and image-guided tumor surgery. *Chem Sci*. 2018;9(12):3105–3110. doi:10.1039/C8SC00206A
14. Yu X, Feng Z, Cai Z, et al. Deciphering of cerebrovasculatures via ICG-assisted NIR-II fluorescence microscopy. *J Mater Chem B*. 2019;7(42):6623–6629. doi:10.1039/C9TB01381D
15. Li Y, Hu X, Yi W, et al. NIR-II fluorescence imaging of skin avulsion and necrosis. *Front Chem*. 2019;7:696. doi:10.3389/fchem.2019.00696
16. Hu Z, Fang C, Li B, et al. First-in-human liver-tumour surgery guided by multispectral fluorescence imaging in the visible and near-infrared-I/II windows. *Nat Biomed Eng*. 2020;4(3):259–271. doi:10.1038/s41551-019-0494-0
17. Debeer S, Le Ludec JB, Kaiserlian D, et al. Comparative histology and immunohistochemistry of porcine versus human skin. *Eur J Dermatol*. 2013;23(4):456–466. doi:10.1684/ejd.2013.2060
18. Ural A, Bilgen F, Aykan DA, et al. Effects of dabigatran and fondaparinux on degloving injuries: an experimental study. *Ulus Travma Acil Cer*. 2020;26(3):343–350.
19. Mothes H, Donicke T, Friedel R, et al. Indocyanine-green fluorescence video angiography used clinically to evaluate tissue perfusion in Microsurgery. *J Trauma*. 2004;57(5):1018–1024. doi:10.1097/01.TA.0000123041.47008.70
20. Moyer HR, Losken A. Predicting mastectomy skin flap necrosis with indocyanine green angiography: the gray area defined. *Plast Reconstr Surg*. 2012;129(5):1043–1048. doi:10.1097/PRS.0b013e31824a2b02
21. He S, Song J, Qu J, Cheng Z. Crucial breakthrough of second near-infrared biological window fluorophores: design and synthesis toward multimodal imaging and theranostics. *Chem Soc Rev*. 2018;47(12):4258–4278. doi:10.1039/C8CS00234G
22. Hong G, Antaris AL, Dai H. Near-infrared fluorophores for biomedical imaging. *Nat Biomed Eng*. 2017;1(1):10. doi:10.1038/s41551-016-0010
23. Antaris AL, Chen H, Diao S, et al. A high quantum yield molecule-protein complex fluorophore for near-infrared II imaging. *Nat Commun*. 2017;8:15269. doi:10.1038/ncomms15269

Clinical, Cosmetic and Investigational Dermatology

Dovepress

Publish your work in this journal

Clinical, Cosmetic and Investigational Dermatology is an international, peer-reviewed, open access, online journal that focuses on the latest clinical and experimental research in all aspects of skin disease and cosmetic interventions. This journal is indexed on CAS. The manuscript management system is completely online and includes a very quick and fair peer-review system, which is all easy to use. Visit <http://www.dovepress.com/testimonials.php> to read real quotes from published authors.

Submit your manuscript here: <https://www.dovepress.com/clinical-cosmetic-and-investigational-dermatology-journal>